3D Stress intensity factor and T-stresses (T$_{11}$ and T$_{33}$) formulations for a Compact Tension specimen

S. K. Kudari

Department of Mechanical Engineering, CVR College of Engineering, Hyderabad, India
s.kudari@rediffmail.com

K. G. Kodancha

Research Centre, Department of Mechanical Engineering, BVB College of Engineering & Technology, Hubli, India
krishnaraja@bvb.edu

ABSTRACT. The paper describes test specimen thickness effect on stress intensity factor (K$_I$), and T-stresses stresses (T$_{11}$ and T$_{33}$) for a Compact Tension specimen. Formulations to estimate 3D K$_I$, T$_{11}$ and T$_{33}$ stresses are proposed based on extensive 3D Finite element analyses. These formulations help to estimate magnitudes of 3D K$_I$ and T$_{11}$ and T$_{33}$ which are helpful to quantify in-plane and out-of- plane constraint effect of the crack tip. The proposed formulations are validated with the similar results available in literature and found to be within acceptable error.

KEYWORDS. Constraint effects; 3D Finite element analysis; Stress intensity factor; T-stress; CT Specimen.

INTRODUCTION

Stress tri-axiality at the crack-tip can alter crack-tip constraint and fracture toughness values of a material. This is the reason transferability of fracture toughness data estimated using laboratory test specimens to a full-scale cracked structure is an important issue in structural integrity assessment of engineering materials. In LEFM non-zero non-singular terms in the series expansion of three-dimensional stress field [1] referred as T-stresses (T$_{11}$ and T$_{33}$) can alter the crack-tip stress tri-axiality and are considered as constraint parameters [2]. T$_{11}$ (the second term of William's extension acting parallel to the crack plane) plays an important role on the in-plane constraint effect. The thickness at the crack tip contributes to the out-of-plane constraint, T$_{33}$ (the second term of William's extension acting along the thickness). To transfer fracture toughness data under different constraints, both in-plane and out-of-plane constraint effect should be considered for the specimens.

Several researchers [3-13] have shown that the specimen thickness has major effect on the magnitude of stress intensity factor and T stresses. Kwon and Sun [7] have presented 3D FE analyses, to investigate the stress fields near the crack-tip and suggested a simple technique to determine 3D K_I at the mid-plane by knowing 2D K_I and Poisson's ratio (υ) of the material using the Eq. (1):

$$\frac{K_{3D}}{K_{2D}} = \sqrt{\frac{1}{1-\upsilon^2}} \tag{1}$$

For quantifications of in-plane and out-of-plane constraint issues, magnitudes of T_{11} and T_{33} stresses are to be computed. But simple formulations such as Eq. (1) to estimate 3D K_I, are not available to compute constraint parameters, T_{11} and T_{33} stresses. Usually they are obtained by complex 3D numerical methods.

The aim of this investigation is to study the variation of K_I, T_{11} and T_{33} along the crack-front considering a CT specimen geometry having varied thickness, B, crack length to width ratio (a/W) and applied stress, σ, using 3D elastic FE analysis. Based on the present finite element results an effort is made to formulate approximate analytical equations to estimate the magnitudes of maximum 3D K_I, T_{11} and T_{33} for a CT specimen. The proposed analytical formulations can be used to estimate the maximum 3D K_I, T_{11} and T_{33} for the CT specimen, which are helpful in quantifying in-plane and out-of-plane constraint issues in fracture. By means of numerical analyses, it is shown that specimen thickness and crack length play an important role on the constraint effects.
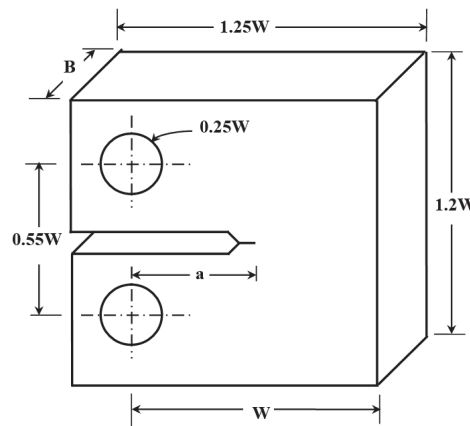

Figure 1: The geometry of the CT specimen used in the analysis (W=20 mm).

FINITE ELEMENT ANALYSIS

Commercial FE software ABAQUS 6.5 [14] is used for the 3D FEA. The dimensions of CT specimen have been chosen according to ASTM standard E1820 [15] and the specimen geometry is shown in the Fig.1. One-half of the specimen geometry is modeled due to specimen symmetry. Twenty noded quadratic brick elements available in the ABAQUS are used to discretize the analysis domain. This kind of elements was used in the earlier works [8, 9] available in the literature. Initially, three-dimensional FE analyses on CT specimens were made by varying number of layers in thickness direction (each layer is of element thickness). It is observed that the variation in results of K_I is insignificant for 8-14 layers. Consequently, in the present analyses 11 layers along the thickness direction were chosen as it gives ten numbers of elements along the thickness direction to extract the K_I and T-stress. Due to half symmetry, the symmetrical boundary conditions have been imposed (u_{x2}=0) along the ligament of the model. Load is applied on approximately 1/3rd portion nodes of the loading-hole circle perpendicular to the ligament. To keep the loading in perfectly Mode-I condition corresponding nodes are arrested except x$_2$-direction. A typical mesh used in the analyses along with boundary conditions is shown in Fig.2. The magnitudes of K_I and T-stresses have been extracted by using ABAQUS post processor. The details of extraction of stress 3D stress intensity factor (K_I) and T-stresses are discussed elsewhere [11,12,16,17]. The variation of K_I and T-stresses along the crack-front has been studied for different specimen thickness (B/W=0.1-1.0) and crack length to width ratio (a/W=0.45-0.70). In this work the magnitude of applied stress, σ, for the CT specimen is computed using the relation [18]:

$$\sigma = \frac{2P(2W + a)}{B(W)^2} \qquad\qquad (2)$$

where, P is applied load, W is width of the specimen, a is crack length. In these finite element calculations, the material behaviour has been considered to be linear elastic pertaining to an interstitial free (IF) steel possessing yield stress σ_y=155MPa, elastic modulus of 197 GPa, Poisson's ratio=0.30.
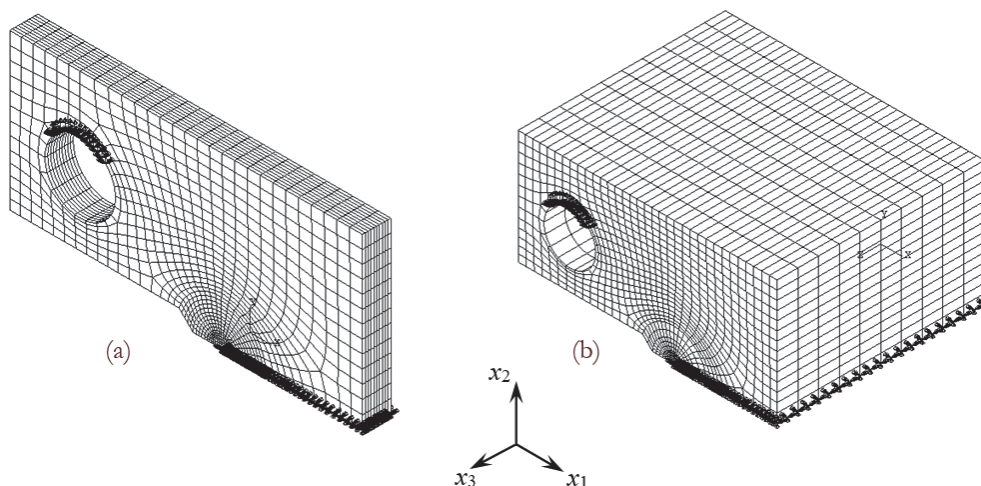

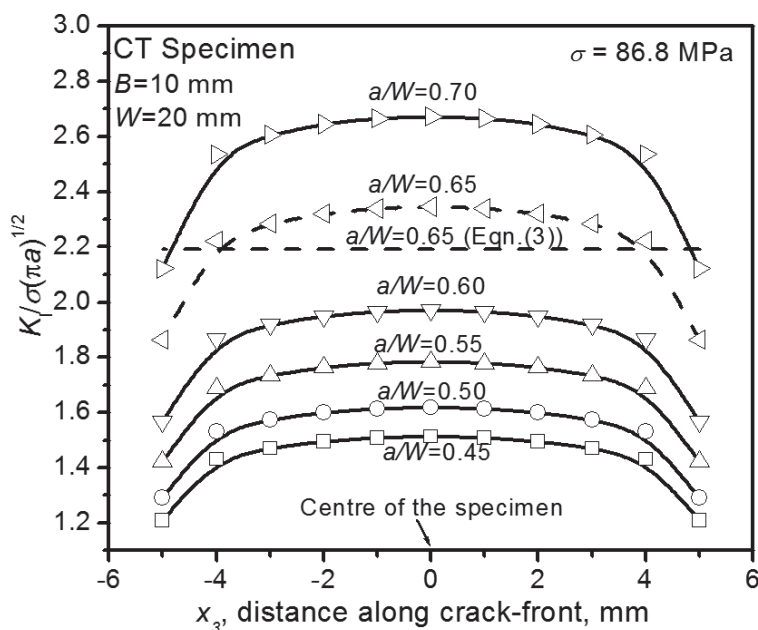Figure 2: 3D CT Specimen mesh along with boundary conditions for a/W=0.50: a) B/W=0.1; b) B/W=1.

Figure 3: Effect of *a/W* on normalized stress intensity factor, $K_I / \sigma(\pi a)^{1/2}$ along crack-front (x₃) for *B*=10mm.

RESULTS AND DISCUSSION

Stress Intensity Factor (K_I)

A typical variation of normalized stress intensity factor ($K_I/\sigma(\pi a)^{1/2}$) and the distance along the crack front (specimen thickness direction, x₃) for specimens having various a/W is shown in Fig.3. The nature of variation of normalized stress intensity factor shown in Fig.3 is in good agreement with the similar results [7,19]. The

magnitudes of 3D maximum stress intensity factors (at the center of the specimen) are compared with the analytical 2D value computed by Eq. (3).

$$K_I = Y\sigma\sqrt{\pi a} \tag{3}$$

Typically, such comparison for a specimen with a/W=0.65 is shown in Fig.3. It is estimated that magnitude of 2D K_I is about 10% lower than 3D K_I.

It is well known that variation of stress intensity factor against $\sigma(\pi a)^{1/2}$ for various specimen thickness (B) is linear, slopes of K_{I-max} vs. $\sigma(\pi a)^{1/2}$ obtained for various a/W are plotted in Fig 4. As the relation between $K_{I-max}/\sigma(\pi a)^{1/2}$ and a/W (Fig.4) is nonlinear, the data is fit with a suitable polynomial. In such exercise, it is found that a polynomial equation of third order fits the 3D FEA results with least error (Regression co-efficient=0.998). This polynomial fit (Eq. (4)) is superimposed on the 3D FEA results plotted in Fig.4 and shows an excellent agreement. From this third order polynomial fit, the relation between K_{I-max}, a/W and σ can be expressed as:

$$\frac{K_{I-max}}{\sigma\sqrt{\pi a}} = 4.48287 - 14.99985\left(\frac{a}{W}\right) + 20.44016\left(\frac{a}{W}\right)^2 - 3.85185\left(\frac{a}{W}\right)^3 \tag{4}$$

Let,

$$C_1 = 4.48287 - 14.99985\left(\frac{a}{W}\right) + 20.44016\left(\frac{a}{W}\right)^2 - 3.85185\left(\frac{a}{W}\right)^3 \tag{5}$$
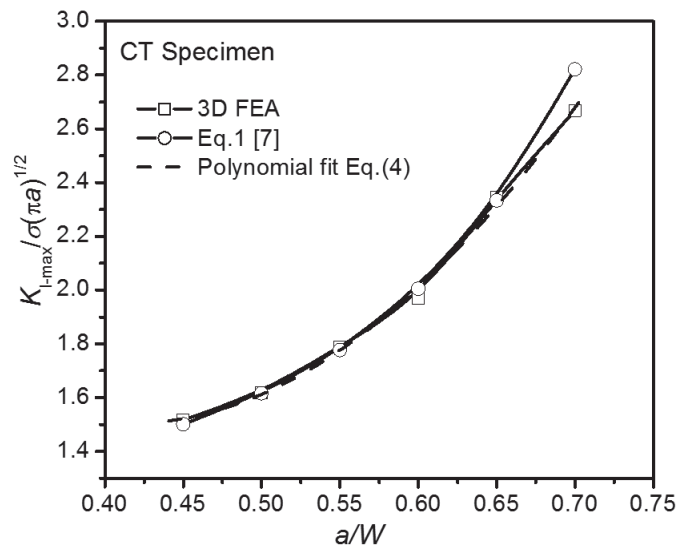

Figure 4: Variation of slopes, $K_{I-max}/\sigma(\pi a)^{1/2}$ vs. a/W.

The Eq. (4) reduces to:

$$K_{I-max} = C_1\sigma\sqrt{\pi a} \tag{6}$$

Eq. (6) is similar to Eq. (3) and the constant C_1 shown in Eq. (5) is similar to the geometric factor, Y as used in Eq. (3). Hence, C_1 in this work is referred as 3D geometric factor. Eq. (6) can be used to estimate magnitudes of K_{I-max} for the CT specimen. To validate the proposed formulation given in Eq. (6), the computed values of K_{I-max} using Eq.(6) for various a/W are compared with the present 3D FEA results and the results computed by Eq.(1) proposed by Kwon and Sun [7] in Fig.4. The figure shows that the results computed by Eq. (6) are in good agreement with the results obtained by

present 3D FEA for a/W 0.45 to 0.70 (entire range of study). The values of K_{I-max} estimated from the Eq.(1) [7] are found to in good agreement with the present results for specimens with a/W 0.45 to 0.65, but for a specimen having a/W>0.65 the Eq.(1) [7] is showing higher error. The error analysis between the results obtained by present 3D FEA and the Eq.(6) is conducted. The maximum percentage of error estimated in use of Eq.(6) for B=2 to 20mm and a/W=0.45 to 0.70 is < 2.95 %.
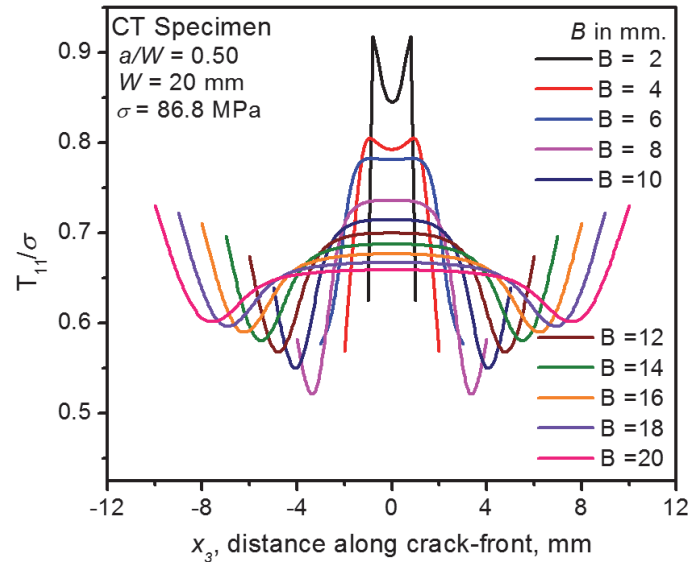

Figure 5: A typical variation of T_{11}/σ along the crack-front for various B and a/W=0.50.

T_{11}-stress

The magnitudes of T_{11} are extracted from 3D FE analysis for varied σ, B and a/W. A typical variation of T_{11} along the crack-front for various B, a/W=0.50 and σ =86.8 MPa is shown in Fig.5. This figure shows that the variation of T_{11} along the crack-front (x_3) depends on the specimen thickness. It is observed that the magnitude of T_{11} is maximum at the centre of the specimen than on the surface. However, for the specimen thickness, B<6mm the maximum value of T_{11} is found to be just below the surface. It is seen from Fig.5 that for specimen with higher thickness, the magnitude of T_{11} decreases for a short distance from the specimen surface and again increases at the centre of the specimen thickness. Similar kind of variation was observed in the work of Pavel et al. [20]. To study the effect of a/W, a typical variation of T_{11}/σ for various a/W, B=10mm and σ =86.8 MPa is plotted in Fig.6. The figure illustrates that T_{11} depends on the specimen a/W, and it is observed to be maximum for higher a/W. The results in Fig.5-6 indicate that the in-plane constraint parameter, T_{11}, is not a unique value (as obtained in 2D analysis) for a specimen thickness, but it varies along the thickness and it is maximum at the centre.

The variation of T_{11} at the center (T_{11-max}) vs. normalized K_I ($K_{I-max}/(\pi B)^{1/2}$) for various specimen thicknesses is studied. A typical plot of T_{11-max} against $K_{I-max}/(\pi B)^{1/2}$ for various a/W and B=10 mm is shown in Fig.7. It is seen from the Fig.7 that the variation of T_{11-max} vs. $K_{I-max}/(\pi B)^{1/2}$ is linear and is independent of a/W. The slopes of T_{11-max} vs. $K_{I-max}/(\pi B)^{1/2}$ are computed for various a/W by fitting a straight-line equation to all the results shown in Fig.7. The estimated slopes $T_{11-max}/(K_{I-max}/(\pi B)^{1/2})$ are plotted against normalized thickness (B/W) for various a/W in Fig. 8. This plot indicates that, the nature of variation of slopes $T_{11max}/(K_{I-max}/(\pi B)^{1/2})$ against B/W is nonlinear and is almost independent of a/W. The result plotted in Fig.8 is used to obtain a relationship between T_{11-max} and K_{I-max}. As there is a small difference is observed in the results presented in Fig.8 for various a/W, the average slope of all a/W for particular B/W is used. The average results are fit by a polynomial equation of third order (Regression Co-efficient=0.994), which give a best fit to all the data. From this third order polynomial fit, the relation between T_{11-max} and K_{I-max} is obtained and can be expressed as:

$$\frac{T_{11-max}}{\left(\frac{K_{I-max}}{\sqrt{\pi B}}\right)} = 0.1477 + 0.93746\left(\frac{B}{W}\right) - 0.87183\left(\frac{B}{W}\right)^2 + 0.35186\left(\frac{B}{W}\right)^3 \qquad (7)$$
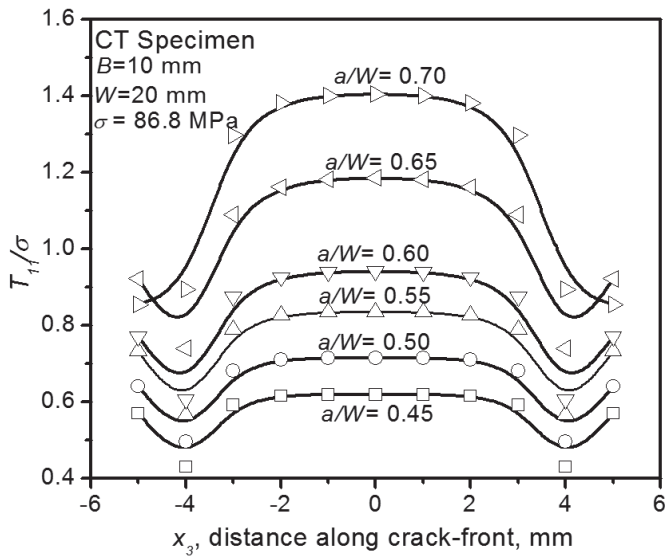
Figure 6: A typical variation of T_{11}/σ along the crack-front for various a/W and B=10mm.

Figure 7: Variation of T_{11-max} against $K_{I-max}/\pi B^{1/2}$ for various a/W and B=10 mm.

Figure 8: Variation of slopes $T_{11-max}/(K_{I-max}/(\pi B)^{1/2}$ against B/W for various a/W.

Let,

$$C_2 = 0.1477 + 0.93746\left(\frac{B}{W}\right) - 0.87183\left(\frac{B}{W}\right)^2 + 0.35186\left(\frac{B}{W}\right)^3 \tag{8}$$

The Eq. (7) reduces to:

$$T_{11-max} = C_2\left(\frac{K_{I-max}}{\sqrt{\pi B}}\right) \tag{9}$$

Substituting for K_{I-max} from Eq.(6)

$$T_{11-max} = C_1.C_2.\sigma\left(\frac{\sqrt{\pi a}}{\sqrt{\pi B}}\right) \tag{10}$$

$$T_{11-max} = C_1.C_2.\sigma\sqrt{\frac{a}{B}} \tag{11}$$

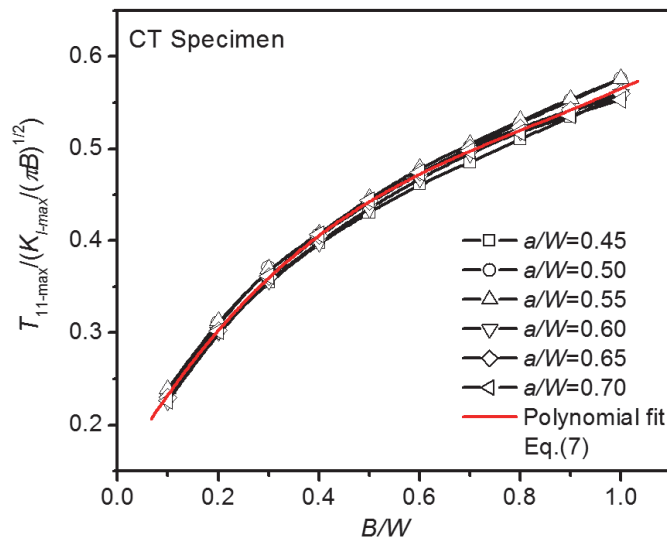where, constant C_1 and C_2 are referred in this work as 3D geometric factors. The values of C_1 for various a/W and C_2 for various B/W for the CT specimen are tabulated in Tab.1 and Tab.2 respectively.

a/W	0.45	0.50	0.55	0.60	0.65	0.70
C_1	1.5211	1.6115	1.7753	2.0094	2.3111	2.6775

Table 1: Values of C_1 computed from Eq.(5).

B/W	0.1	0.2	0.3	0.4	0.5	0.6	0.7	0.8	0.9	1.0
C_2	0.2331	0.3031	0.3600	0.4057	0.4425	0.4723	0.4974	0.5199	0.5417	0.5652

Table 2: Values of C_2 computed from Eq.(8).

The above Eq.(11) can be used to estimate T_{11-max} for the CT specimen for a given specimen dimensions and applied load, σ. A typical plot of T_{11-max} computed from Eq.(11) is superimposed (Red curve) on 3D FEA results shown in Fig. 8. This plot shows a good agreement with the results estimated by Eq.(11) and 3D FEA. An error analysis is carried out between the estimated values from Eq.(11) and the present 3D FEA results. The maximum percentage of error in use of Eq.(11) for various B, a/W and σ used in this study is found to be < 5.1%. The proposed analytical Eq.(11) is a simple method to compute T_{11-max} for the CT specimen geometry.
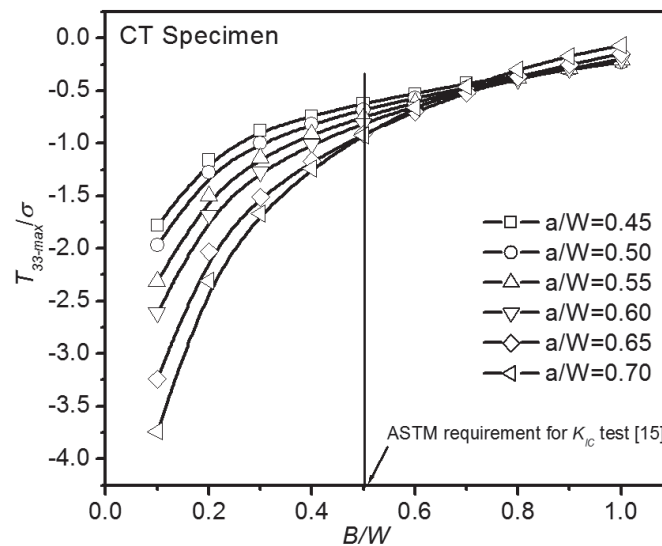

Figure 9: Variation of T_{33}/σ against B/W for various a/W.

T_{33}-stress

The magnitudes of T_{33} are estimated using Eq.(12) by substituting the extracted ε_{33} (strain) from ABAQUS post processor and T_{11} for varied σ, B and a/W.

$$T_{33} = E\varepsilon_{33} + \upsilon T_{11} \tag{12}$$

The variation of $T_{33\text{-max}}/\sigma$ against B/W for various a/W is shown in Fig.9. This figure indicates that, T_{33} strongly depend on B/W. It is observed that the magnitude of T_{33} is negative for all cases that were considered in this analysis, and approached to zero as B/W increased to 1. For B/W=0.5, ASTM requirement for K_{IC} test specimen [15], it is seen that T_{33}/σ is negative indicating loss of out-of-plane constraint. T_{33} also showed dependence on a/W, for B/W<0.7, T_{33} is found to be maximum for thinner specimens (B/W=0.1) with higher a/W =0.7. As T_{33} strongly depends on the specimen thickness, it is not possible to get a simple relation between T_{33} and specimen geometry as obtained in case of K_I and T_{11}. To obtain expressions between T_{33}, specimen geometry and the applied load, the results in Fig.9 are given a polynomial fit to suit the 3D FEA results. In this exercise, it is found that the 5th order polynomial fits the data with least error. A typical equation for estimation of $T_{33\text{-max}}$ is given by Eq. (13). The equations for the 3D geometric factors (C_3) to compute $T_{33\text{-max}}$ for various a/W obtained by fitting 5th order polynomial are tabulated in Tab.3.

$$T_{33\text{-max}} = C_3\sigma \tag{13}$$

The computed values of C_3 for various a/W are given in Tab.4. The maximum percentage of error in the use of equations given in Tab.3 for various B, a/W and σ is found to be < 7.8%.

a/W	Polynomial Equations
0.45	$\dfrac{T_{33-\max}}{\sigma} = -3.02667 + 16.98748\left(\dfrac{B}{W}\right) - 53.07517\left(\dfrac{B}{W}\right)^2 + 86.44814\left(\dfrac{B}{W}\right)^3 - 68.70629\left(\dfrac{B}{W}\right)^4 + 21.15385\left(\dfrac{B}{W}\right)^5$
0.50	$\dfrac{T_{33-\max}}{\sigma} = -3.32333 + 18.49597\left(\dfrac{B}{W}\right) - 58.0134\left(\dfrac{B}{W}\right)^2 + 95.41084\left(\dfrac{B}{W}\right)^3 - 76.51515\left(\dfrac{B}{W}\right)^4 + 23.71795\left(\dfrac{B}{W}\right)^5$
0.55	$\dfrac{T_{33-\max}}{\sigma} = -3.858 + 20.88005\left(\dfrac{B}{W}\right) - 62.97348\left(\dfrac{B}{W}\right)^2 + 100.77273\left(\dfrac{B}{W}\right)^3 - 79.1317\left(\dfrac{B}{W}\right)^4 + 24.10256\left(\dfrac{B}{W}\right)^5$
0.60	$\dfrac{T_{33-\max}}{\sigma} = -4.40067 + 24.26372\left(\dfrac{B}{W}\right) - 74.31294\left(\dfrac{B}{W}\right)^2 + 121.11772\left(\dfrac{B}{W}\right)^3 - 96.8648\left(\dfrac{B}{W}\right)^4 + 30\left(\dfrac{B}{W}\right)^5$
0.65	$\dfrac{T_{33-\max}}{\sigma} = -5.582 + 31.84602\left(\dfrac{B}{W}\right) - 98.58275\left(\dfrac{B}{W}\right)^2 + 162.16142\left(\dfrac{B}{W}\right)^3 - 130.62937\left(\dfrac{B}{W}\right)^4 + 40.64103\left(\dfrac{B}{W}\right)^5$
0.70	$\dfrac{T_{33-\max}}{\sigma} = -6.44533 + 36.53654\left(\dfrac{B}{W}\right) - 110.79021\left(\dfrac{B}{W}\right)^2 + 181.22902\left(\dfrac{B}{W}\right)^3 - 146.36364\left(\dfrac{B}{W}\right)^4 + 45.76923\left(\dfrac{B}{W}\right)^5$

Table 3: Polynomial equations for T_{33}.

a/W	B/W									
	0.1	0.2	0.3	0.4	0.5	0.6	0.7	0.8	0.9	1.0
0.45	-1.7789	-1.1638	-0.8782	-0.7333	-0.6288	-0.5279	-0.4316	-0.3537	-0.2952	-0.2187
0.50	-1.9659	-1.2962	-0.9818	-0.8167	-0.6934	-0.5739	-0.4618	-0.3735	-0.3097	-0.2271
0.55	-2.3066	-1.5136	-1.1231	-0.9112	-0.7573	-0.6148	-0.4825	-0.3758	-0.2971	-0.2078
0.60	-2.6057	-1.6969	-1.2512	-1.0063	-0.8239	-0.6545	-0.5012	-0.3831	-0.3003	-0.1970
0.65	-3.2337	-2.0548	-1.4816	-1.1664	-0.9288	-0.7066	-0.5075	-0.3600	-0.2647	-0.1457
0.70	-3.7325	-2.3393	-1.6366	-1.2367	-0.9384	-0.6721	-0.4449	-0.2855	-0.1895	-0.0644

Table 4: Values of C_3 computed from formulations given in Tab.3.

To evaluate the worthiness of the analytical expressions to estimate $K_{I\text{-max}}$, $T_{11\text{-max}}$ and $T_{33\text{-max}}$ proposed in this analysis, the estimated magnitudes $K_{I\text{-max}}$, $T_{11\text{-max}}$ and $T_{33\text{-max}}$ obtained by Eq.(6), Eq.(11) and Tab.3 are compared with the similar results on the CT specimen presented by Toshiyuki and Tomohiro [12]. The authors [12] have given the variation of $T_{11\text{-max}}$ and $T_{33\text{-max}}$ for the toughness value of the material (0.55% Carbon Steel) $K_{I\text{-max}}$= 66 MPam$^{1/2}$. Fig. 10 shows a typical variation of estimated $K_{I\text{-max}}$, $T_{11\text{-max}}$ and $T_{33\text{-max}}$ at the specimen thickness center against B/W (0.1 -1.0) obtained by proposed analytical expressions (Eq.(6), (11) and Tab.3) for $K_{I\text{-max}}$= 66 MPam$^{1/2}$ and results of Toshiyuki and Tomohiro [12]. The authors [12] have computed various parameters for B/W=0.25, 0.4 and 0.5 only. According to Fig. 10, the magnitudes of $K_{I\text{-max}}$ were not affected by B/W as expected and are in excellent agreement with Toshiyuki and Tomohiro [12]. T_{11} showed visible dependence on B/W, though the variation was less than 20% and it is in good agreement with the earlier reported results [12]. In summary, the in-plane parameters at the specimen thickness center showed small dependence on B, and are in excellent agreement with the earlier results [12] providing validation for the proposed Eq.(6) and (11). On the other hand, out-of-plane constraint factor, T_{33} showed strong dependence on B/W. T_{33} was found negative and approached zero as B/W increased from 0.1 to 1. Fig. 10 shows that the nature of variation of present results of T_{33} (obtained by Tab.3 expressions) is in similar manner to the one presented by Toshiyuki and Tomohiro [12]. However, some difference in the magnitude of T_{33} between both the results for B/W=0.25-0.5 is observed. This difference is attributed to the effect of side grooves in the CT specimen used in the work of Toshiyuki and Tomohiro [12]. The side grooves in the specimen affects the strain distribution in the out-of-plane direction and restricts the value of T_{33} (Ref. Eq.(12)). To study this effect, we have conducted 3D FEA on CT specimen used by Toshiyuki and Tomohiro [12] without side groove and for the same material properties. These computed results are superimposed in Fig.10 by red colored lines for comparison. This plot show that the results ($K_{I\text{-max}}$, $T_{11\text{-max}}$ and $T_{33\text{-max}}$) for the specimen without side groove match with the one computed by the analytical expressions (Eq.(6), (11) and Tab.3) proposed in this work. This exercise infers that the use of side grooves in a specimen controls ε_{33} and improves the out-of-plane constraint (Ref.Fig.10: for a/W=0.5, T_{33} is improved from -150 MPa to -84 MPa (44%) by using 10% side groove [12]). The Fig. 10 provides validation to the proposed analytical formulations to estimate $K_{I\text{-max}}$, $T_{11\text{-max}}$ and $T_{33\text{-max}}$.
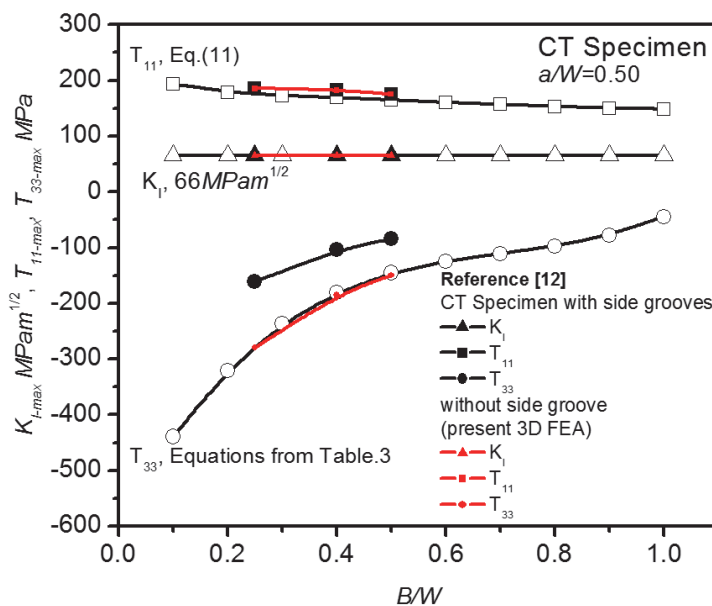

Figure 10: A typical variation of $K_{I\text{-max}}$, $T_{11\text{-max}}$ and $T_{33\text{-max}}$ against B/W obtained by proposed analytical expressions and results of Toshiyuki and Tomohiro [12].

SUMMARY

In this study, stress intensity factor and T-stress (T_{11} and T_{33}) solutions for CT specimens for wide range of specimen thickness and crack lengths were computed using 3D elastic FEA. It is observed that magnitude of T_{33} (Ref: Fig.(9)) is highly negative for B/W=0.1 (thin specimens), and almost zero for B/W=1 (thick specimens), indicating that the thick specimens have higher out-of-plane constraint. For B/W=0.5, ASTM requirement for K_{IC} test [15], it is observed

that T_{33}/σ is negative indicating some loss of out-of-plane constraint. For the specimens with similar a/W and B/W the loss of out-of-plane constraint (T_{33}) is much significant than the in plane constraint (T_{11}) (Ref. Fig.10). This infers that the major constraint loss in a CT specimen is due to the out-of-plane effects. The out-of-plane constraint loss can be corrected to some extent by providing side grooves to a CT specimen. Using the present 3D FEA results, approximate analytical formulations are proposed to evaluate the K_{I-max}, T_{11-max} and T_{33-max} by knowing only applied stress and specimen dimensions. These formulations can be helpful in the analysis of in-plane and out-of-plane constraint issues.

REFERENCES

[1] Nakamura, T., Parks, D. M., Determination of elastic T-stress along three-dimensional crack fronts using an interaction integral, Int. J. Solids Struct., 29 (1992) 1597–1611.
[2] Betegon, C., Hancock, J. W., Two-parameter characterization of elastic–plastic crack tip fields, J Appl Mech., 58 (1991) 104–110.
[3] Kudari, S. K., Kodancha, K. G., A new formulation for estimating maximum stress intensity factor at the mid plane of a SENB specimen: Study based on 3D FEA, Frattura ed Integrità Strutturale, 29 (2014) 419-425.
[4] Nakamura, T., Parks, D. M., Three-dimensional crack front fields in a thin ductile plate, J. Mech. Phys. Solids., 38 (1990) 787–812.
[5] Nevalainen, M., Dodds, R. H., Numerical investigation of 3-D constraint effects on brittle fracture in SE(B) and C(T) specimens, Int. J. Fract., 74 (1995) 131–161.
[6] Leung, A. Y. T., Su, R.K.L., A numerical study of singular stress field of 3D cracks, Finite Elem. Anal. Design., 18 (1995) 389–401.
[7] Kwon, S. W., Sun, C.T., Characteristics of three-dimensional stress fields in plates with a through -the-thickness crack, Int. J. Fract., 104 (2000) 291-315.
[8] Jie, Q., Xin, W., Solutions of T-stresses for quarter-elliptical corner cracks in finite thickness plates subject to tension and bending, Int. J. Pres. Ves. Pip., 83 (2006) 593–606.
[9] Moreira, P. M. G. P., Pastrama, S. D., Castro, P. M.. S. T., Three-dimensional stress intensity factor calibration for a stiffened cracked plate, Engng. Fract. Mech., 76 (2009) 298–2308.
[10] Kodancha, K. G., Kudari, S. K., Variation of stress intensity factor and elastic T-stress along the crack-front in finite thickness plates. Frattura ed Integrità Strutturale, 8 (2009) 45-51.
[11] Toshiyuki, M., Tomohiro, T., Kai, L., T-stress solutions for a semi-elliptical axial surface crack in a cylinder subjected to mode-I non-uniform stress distributions, Engng. Fract. Mech., 77 (2010) 2467-2478.
[12] Toshiyuki, M., Tomohiro, T., Experimental T_{33}-stress formulation of test specimen thickness effect on fracture toughness in the transition temperature region, Engng. Fract. Mech., 77 (2010) 867-877.
[13] Kai, L., Toshiyuki, M., Three-dimensional T-stresses for three-point-bend specimens with large thickness Variation, Engng. Fract. Mech., 116 (2014) 197-203
[14] ABAQUS V 6.5-1. (2004) Hibbitt, Karlsson & Sorensen, Inc.
[15] American Society for Testing and Materials., Standard Test Method for Measurement of Fracture Toughness, (2015) ASTM E1820-15a.
[16] Moran, B., Shih, C. F., Crack tip and associated domain integrals from momentum and energy balance. Engng. Fract. Mech., 27 (1987) 615-642.
[17] Gosz, M., Dolbow, J., Moran, B., Domain integral formulation for stress intensity factor computation along curved three-dimensional interface cracks. Int. J Solids Struct., 35 (1998) 1763-1783.
[18] Priest, A. H., Experimental methods for fracture toughness measurement, J. Strain Analysis, 10 (1975) 225-232.
[19] Fernandez, Z. D., Kalthoff, J. F., Fernandez, C. A ,Canteli, A., Grasa, J., Doblare, M. Three dimensional finite element calculations of crack-tip plastic zones and K_{IC} specimen size requirements, ECF-15, (2005)
[20] Pavel, H., Martin, S., Lubos, N., Michal, Z., Stanislav, S., Zdenek, K., Alfonso, F. C., Fracture mechanics of the three-dimensional crack front: vertex singularity versus out of plain constraint descriptions, Procedia Engng., 2 (2010) 2095-2102.